

This is the accepted manuscript made available via CHORUS. The article has been published as:

In-plane magnetic penetration depth of superconducting $\text{CaKFe}_{4}\text{As}_{4}$

Rustem Khasanov, William R. Meier, Yun Wu, Daixiang Mou, Sergey L. Bud'ko, Ilya Eremin,
Hubertus Luetkens, Adam Kaminski, Paul C. Canfield, and Alex Amato

Phys. Rev. B **97**, 140503 — Published 9 April 2018

DOI: [10.1103/PhysRevB.97.140503](https://doi.org/10.1103/PhysRevB.97.140503)

In-plane magnetic penetration depth of superconducting $\text{CaKFe}_4\text{As}_4$

Rustem Khasanov,^{1,*} William R. Meier,^{2,3} Yun Wu,^{2,3} Daixiang Mou,^{2,3} Sergey L. Bud'ko,^{2,3} Ilya Eremin,⁴ Hubertus Luetkens,¹ Adam Kaminski,^{2,3} Paul C. Canfield,^{2,3} and Alex Amato¹

¹*Laboratory for Muon Spin Spectroscopy, Paul Scherrer Institut, CH-5232 Villigen PSI, Switzerland*

²*Division of Materials Science and Engineering, Ames Laboratory, Ames, Iowa 50011, USA*

³*Department of Physics and Astronomy, Iowa State University, Ames, Iowa 50011, USA*

⁴*Institut für Theoretische Physik III, Ruhr-Universität Bochum, 44801 Bochum, Germany*

The temperature dependence of the in-plane magnetic penetration depth (λ_{ab}) in an extensively characterized sample of superconducting $\text{CaKFe}_4\text{As}_4$ ($T_c \simeq 35$ K) was investigated using muon-spin rotation (μSR). A comparison of $\lambda_{ab}^{-2}(T)$ measured by μSR with the one inferred from ARPES data confirms the presence of multiple gaps at the Fermi level. An agreement between μSR and ARPES requires the presence of additional bands, which are not resolved by ARPES experiments. These bands are characterised by small superconducting gaps with an average zero-temperature value of $\Delta_0 = 2.4(2)$ meV. Our data suggest that in $\text{CaKFe}_4\text{As}_4$ the s^\pm order parameter symmetry acquires a more sophisticated form by allowing a sign change not only between electron and hole pockets, but also within pockets of similar type.

PACS numbers: 74.70.Xa, 74.25.Bt, 74.45.+c, 76.75.+i

Since their discovery, iron based superconductors (Fe-SC's) have attracted much interest. This broad class of materials exhibits unconventional superconducting properties, due to the strong interplay of superconductivity with various electronic ground states, including a nematic phase and spin-density wave magnetism.^{1–5} Recently a new Fe-SC family was synthesized, namely $\text{AeAFe}_4\text{As}_4$ ($\text{Ae} = \text{Ca, Sr, Eu}$ and $A = \text{K, Rb, Cs}$), with superconducting transition temperature (T_c) reaching $\simeq 36$ K.^{6,7} $\text{CaKFe}_4\text{As}_4$ (CaK1144) is currently the most studied representative of the AeA1144 Fe-SC family with $T_c \simeq 35$ K and an estimated upper critical field $H_{c2}^\perp \simeq 92$ T.^{6,7} High-resolution angular resolved photoemission (ARPES), nuclear magnetic resonance, tunneling and penetration depth measurements,^{8–12} as well as density functional theory (DFT) calculations^{8,13} support multiband superconductivity in $\text{CaKFe}_4\text{As}_4$ with Cooper pairing occurring in electron- and hole-like bands.

In spite of the good agreement between results obtained by different techniques, the gap structure as well as the gap magnitudes are still not conclusively determined. DFT calculations suggest that ten bands cross the Fermi level (6 hole- and 4 electron-like bands).^{8,13} ARPES experiments, on the other hand, reveal only the presence of four bands (α -, β -, γ -, and δ -bands) with nearly isotropic superconducting energy gaps, with the corresponding zero-temperature values of $\Delta_{0,\alpha} = 10.5$, $\Delta_{0,\beta} = 13$, $\Delta_{0,\delta} = 8$, and $\Delta_{0,\gamma} = 12$ meV.⁸ Tunneling experiments show that the superconducting gaps are spread between 1 and 10 meV with a broad peak appearing at around 3 meV, while the superfluid density measurements suggest nodeless two-gap superconductivity with a larger gap of $\sim 6 - 10$ meV and a smaller gap of $\sim 1 - 4$ meV.^{9,10,12}

In this paper, we report on measurements of the in-plane magnetic penetration depth (λ_{ab}) and the vortex core size (ξ_{ab}) in a $\text{CaKFe}_4\text{As}_4$ single crystal sample by means of the muon-spin rotation (μSR) technique. The

obtained temperature dependence of λ_{ab} was compared with the calculations based on the analysis of the electronic band structure and the momentum dependent superconducting gap extracted from the ARPES data. An agreement between the results obtained by both techniques requires the presence of additional bands which were not resolved in ARPES experiments.

$\text{CaKFe}_4\text{As}_4$ single crystals were grown from a high-temperature Fe-As rich melt and extensively characterized via thermodynamic and transport measurements.⁷ A fraction of the ARPES data was previously reported in Ref. 8. A crystal with dimensions of $\simeq 4.0 \times 4.0 \times 0.1$ mm³ was used for the μSR experiments, which were carried out at the πM3 beam line using the GPS spectrometer (Paul Scherrer Institute, Switzerland).¹⁴ Transverse-field (TF) μSR measurements were performed at temperatures from $\simeq 1.5$ to 50 K. The external magnetic field (H_{ap}) ranging from 5 to 580 mT was applied along the crystallographic c -axis of the crystal. A spin rotator was used to orient the initial spin polarization of the muon beam at 45° degrees with respect to the applied field. A special sample holder designed to measure thin samples by means of μSR was used.¹⁵ The experimental data were analyzed using the MUSRFIT package.¹⁶

Figure 1 shows the Fourier transform of TF- μSR time spectra reflecting the internal field distribution $P(B)$ in the $\text{CaKFe}_4\text{As}_4$ single crystal sample. The results of field-cooled measurements in a field of $\mu_0 H_{\text{ap}} = 30$ mT (panel a) and 580 mT (panel b) above ($T = 42.2$ K) and below ($T = 1.55$ K) $T_c \simeq 35$ K are presented. The asymmetric $P(B)$ distributions at $T = 1.55$ K possess the basic features expected for an ordered vortex lattice, namely: the cutoff at low fields, the peak shifted below H_{ap} , and the long tail towards the high field direction (see *e.g.* Refs. 15,17 and references therein). The sharp peak at $B = \mu_0 H_{\text{ap}}$ represents the residual background signal from muons missing the sample. The μSR time spectra were analyzed using a three compo-

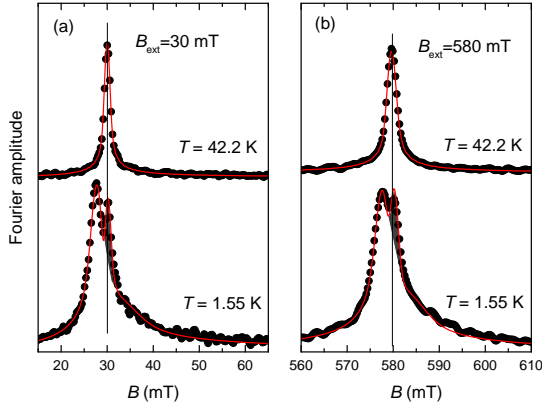


FIG. 1: Fourier transform of the TF- μ SR time spectra obtained in an applied field of $\mu_0 H_{\text{ap}} = 30$ mT (a) and $\mu_0 H_{\text{ap}} = 580$ mT (b) above ($T = 42.2$ K) and below ($T = 1.55$ K) $T_c \simeq 35$ K. Red lines are the two ($T = 42.2$ K) and three ($T = 1.55$ K) component Gaussian fits corresponding to the field distribution $P(B)$ described by Eq. 1. The peak at $B = \mu_0 H_{\text{ap}}$ represents the background signal.

nent Gaussian expression with the first (the temperature and field independent) component corresponding to the background contribution, and another two components accounting for the asymmetric $P(B)$ distribution in the mixed state of superconductor (see the Supplemental Information, Ref. 18, and Refs. 24,25 for details). The time-domain expression is equivalent to a distribution in the field-domain:

$$P(B) = P(B)_b + P(B)_s = \frac{\gamma_\mu A_b}{\sigma_b} \exp\left(-\frac{\gamma_\mu^2 (B - B_b)^2}{2\sigma_b^2}\right) + \sum_{i=1}^2 \frac{\gamma_\mu A_i}{\sigma_i} \exp\left(-\frac{\gamma_\mu^2 (B - B_i)^2}{2\sigma_i^2}\right). \quad (1)$$

Indexes b and s correspond to the background and the sample contributions, respectively. $A_b(A_i)$, $\sigma_b(\sigma_i)$, and $B_b(B_i)$ are the asymmetry, the relaxation rate, and the mean field of the background (i -th sample) component. $\gamma_\mu = 2\pi \times 135.5342$ MHz/T is the muon gyromagnetic ratio. For $T \geq T_c$ the analysis of the sample contribution was simplified to a single Gaussian lineshape.

The first moment ($\langle B \rangle$), the second- ($\langle \Delta B^2 \rangle$) and third-central moments ($\langle \Delta B^3 \rangle$) of $P(B)_s$ were obtained analytically (see the Supplemental Information, Ref. 18) and have the following physical interpretations: (i) The first moment (the mean field) is generally smaller than H_{ap} , due to the diamagnetic nature of the superconducting state. The field shift $\mu_0 H_{\text{ap}} - \langle B \rangle$ scales with the sample magnetization.²⁶ (ii) The second moment encodes the broadening of the signal, and contains contributions from the vortex lattice and the nuclear dipole field. The assumedly temperature independent nuclear dipolar field contribution (σ_{nm}) is determined from measurements made above T_c . The superconducting component ($\langle \Delta B^2 \rangle_s$) is then obtained by subtracting σ_{nm} from

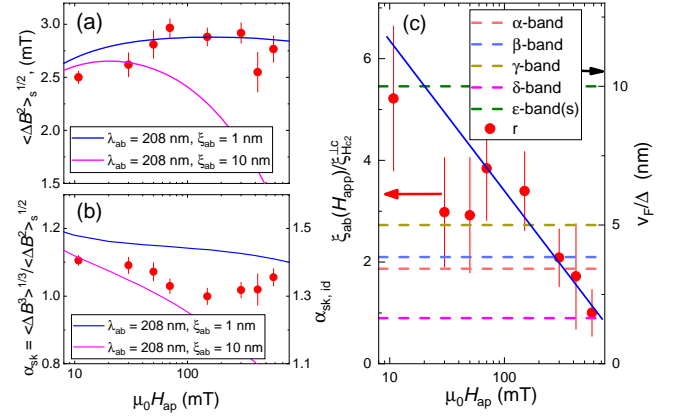


FIG. 2: (a) Field dependence of $\langle \Delta B^2 \rangle_s^{1/2}$ of $\text{CaKFe}_4\text{As}_4$ at $T = 1.55$ K. (b) Dependence of α_{sk} on H_{ap} . The pink and blue solid lines in (a) and (b) are calculations obtained within the framework of the London model with Gaussian cut-off for $\lambda_{ab} = 208$ nm, $\xi_{ab} = 10$ nm and $\lambda_{ab} = 208$ nm, $\xi_{ab} = 1$ nm, respectively. (c) Dependence of $\xi_{ab}/\xi_{H_{c2}}^{1/2}$ on H_{ap} . Dashed lines correspond to $\langle v_F \rangle_i / \Delta_{0,i}$ values ($i = \alpha, \beta, \gamma, \delta$, or ϵ is the band index).

the measured second moment: $\langle \Delta B^2 \rangle_s = \langle \Delta B^2 \rangle - \sigma_{\text{nm}}^2$. $\langle \Delta B^2 \rangle_s$ is a function of the magnetic penetration depth λ and the vortex core size $\xi \sim \xi_{H_{c2}}$ ($\xi_{H_{c2}}$ is the coherence length as obtained from the upper critical field). In extreme type-II superconductors ($\lambda \gg \xi_{H_{c2}}$) and for fields much smaller than the upper critical field $\langle \Delta B^2 \rangle_s$ is proportional to λ^{-4} .^{27,28} (iii) The third moment accounts for the asymmetric shape of $P(B)$, which is described via the skewness parameter $\alpha_{\text{sk}} = \langle \Delta B^3 \rangle^{1/3} / \langle \Delta B^2 \rangle_s^{1/2}$. In the limit of $\lambda \gg \xi$ and for realistic measurement conditions $\alpha_{\text{sk}} \simeq 1.2$ for a well arranged triangular vortex lattice. It is very sensitive to structural changes of the vortex lattice which may occur as a function of temperature and/or magnetic field.^{29,30}

Figures 2 (a) and (b) show the dependence of the square root of the second moment $\langle \Delta B^2 \rangle_s^{1/2}$ and the skewness parameter α_{sk} on H_{ap} at $T = 1.55$ K. Since in our experiments the magnetic field was applied along the crystallographic c -axis, both $\langle \Delta B^2 \rangle_s^{1/2}$ and α_{sk} are functions of the in-plane components of the magnetic penetration depth (λ_{ab}) and the vortex core size (ξ_{ab}). The experimental data were compared with calculations performed within the framework of the London model with Gaussian cut-off for an ideal hexagonal vortex lattice (see the Supplemental part, Ref. 18 and Refs. 27,31–33).

The analysis reveals that both experimental $\langle \Delta B^2 \rangle_s^{1/2}$ and α_{sk} field dependencies can be described with an essentially field independent $\lambda_{ab} \simeq 208$ nm and ξ_{ab} ranging from $\simeq 1$ to 10 nm. As an example, solid curves in Figs. 2 (a) and (b) correspond to the theory calculations for an ideal vortex lattice with $\lambda_{ab} = 208$ nm, $\xi_{ab} = 10$ nm (pink curve) and $\lambda_{ab} = 208$ nm, $\xi_{ab} = 1$ nm (blue curve).

Note that due to vortex lattice distortions, which are always present in real superconducting samples, the experimentally observed α_{sk} is slightly smaller than the ideal value $\alpha_{\text{sk,id}}$ obtained after calculations.¹⁷ The independence of λ on the magnetic field is a characteristic feature of fully gapped superconductors. As shown by Kadono,³⁴ λ increases with increasing field if the superconducting gap contains nodes and is field independent if the gap is isotropic. Our results suggest, therefore, that $\text{CaKFe}_4\text{As}_4$ is a nodeless superconductor in good agreement with the previously reported data.^{8–10,12}

According to Fente *et al.*¹⁰, the vortex core size in $\text{CaKFe}_4\text{As}_4$ decreases with increasing field. Our experimental data are consistent with this finding. Figures 2 (a) and (b) imply that the low-field $\langle B^2 \rangle_s^{1/2}$ and α_{sk} points stay closer to the $\xi_{ab} = 10$ nm theory curves, while the high field values are closer to $\xi_{ab} = 1$ nm curves. The field-induced decrease of ξ_{ab} also accounts for the local minimum on $\alpha_{\text{sk}}(H_{\text{ap}})$ at $\mu_0 H_{\text{ap}} \simeq 150$ mT [see Fig. 2 (b)]. Under the assumption of field independent $\lambda_{ab} = 208(4)$ nm and $\xi_{ab}(0.58 \text{ T}) = \xi_{\text{Hc}2}^{\perp c}$ ($\xi_{\text{Hc}2}^{\perp c} = 1.43$ nm is the coherence length as obtained from the upper critical field, Ref. 7) the field dependence of $\xi_{ab}(H_{\text{ap}})/\xi_{\text{Hc}2}^{\perp c}$ was reconstructed [see Fig. 2 (c) and the Supplemental Information for details, Ref. 18].

TABLE I: Parameters extracted and calculated from ARPES and μSR data. $\Delta_{0,i}$ is the zero-temperature value of the superconducting gap, $\langle v_F \rangle_i$ is the mean value of the Fermi velocity, $\langle d_F \rangle_i$ is the average diameter of the Fermi surface sheet, and $\lambda_{ab,i}^{-2}(0)/\lambda_{ab}^{-2}(0)$ is the relative contribution of i -th band to $\lambda_{ab}^{-2}(0)$.

	$\Delta_{0,i}$ (meV)	$\langle v_F \rangle_i$ (eV·nm)	$\langle d_F \rangle_i$ (nm ⁻¹)	$\frac{\lambda_{ab,i}^{-2}(0)}{\lambda_{ab}^{-2}(0)}$	Technique
α -band	10.5(0.8)	0.036(1)	1.60(25)	0.073(11)	ARPES
β -band	13.0(0.8)	0.050(2)	3.23(25)	0.202(15)	
γ -band	8.0(0.6)	0.040(1) ^a	6.53(25)	0.323(12)	
δ -band	12.0(1.3)	~ 0.008	3.30(25)	0.032(3)	
ϵ -bands	2.4(2)	~ 0.025	~ 10.0 ^b	0.370(40)	μSR

^aAveraged over $h\nu = 6.7$ and 21.2 eV photon energies, Fig. 3.

^bThe sum of diameters.

The decrease of the vortex core size with increasing field was observed in various conventional and unconventional superconductors in tunneling, magnetisation and μSR experiments (see *e.g.* Refs. 35–38) as well as reported for $\text{CaKFe}_4\text{As}_4$ in tunneling experiments for fields exceeding 0.5 T.¹⁰ The strongest effect was observed in multigap superconductors like MgB_2 , NbSe_2 ^{36,39} and it was explained by the gap and Fermi velocity dependent length scales $\xi_i \propto \langle v_F \rangle_i / \Delta_{0,i}$ (i is the band index and $\langle v_F \rangle$ is the mean value of the Fermi velocity). At low and high magnetic fields the vortex core size is governed by the high and the low $\langle v_F \rangle_i / \Delta_{0,i}$ ratios, respectively. Previous ARPES experiments on $\text{CaKFe}_4\text{As}_4$ reveal the presence of at least four bands crossing the Fermi level with the corresponding Δ_0 values summarized in Table I.⁸ Fermi

velocities were further obtained in this work by performing linear fits of the band dispersion curves near the Fermi energy (see Fig. 3 and Table I). Obviously, the four bands reported in ARPES experiments do not explain the $\xi_{ab}/\xi_{\text{Hc}2}^{\perp c}$ vs. H_{ap} behavior shown in Fig. 2 (c). One needs to assume the presence of an additional band, or series of bands (ϵ -bands), with $\langle v_F \rangle_\epsilon / \Delta_{0,\epsilon} \simeq 10$ nm. Bearing in mind that a small gap of $\Delta_{0,\epsilon} \simeq 2.4$ meV was obtained in our $\lambda_{ab}^{-2}(T)$ studies (see the following discussion), as well as reported in tunneling and superfluid density experiments by other groups,^{9,10,12} the average Fermi velocity within the ϵ -bands is $\langle v_F \rangle_\epsilon \simeq 0.025$ eV·nm. This value is well within the range for $\langle v_F \rangle$'s obtained by ARPES (see Table I).

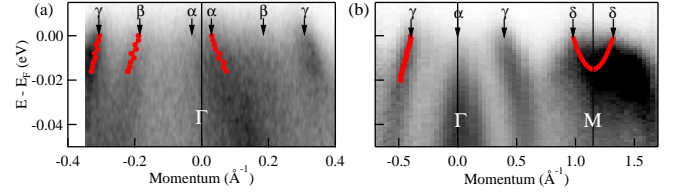


FIG. 3: Band dispersions of $\text{CaKFe}_4\text{As}_4$ at $T = 40$ K obtained in ARPES experiments: (a) by using the laser light source at the photon energy $h\nu = 6.7$ eV; (b) by using plasma Helium lamp with $h\nu = 21.2$ eV. Red lines are fits of the band dispersion curves near zero-energy allowing to obtain the Fermi velocities. The units of momentum are kept in \AA^{-1} for consistency with ARPES works.

Fig. 4 (a) compares the $\lambda_{ab}^{-2}(T)$ dependence obtained in μSR experiment from the measured $\langle B^2 \rangle^{1/2}$ at $\mu_0 H = 11$ mT (red open circles) with the one calculated from the electronic band dispersion and the momentum resolved superconducting gap measured by ARPES. Following Refs. 40–43, $\lambda_{ab}^{-2}(T)$ is determined as:

$$\lambda_{ab}^{-2}(T) = \sum_i I_i \left[1 + 2 \int_{\Delta_i(T)}^{\infty} \left(\frac{\partial f}{\partial E} \right) \frac{E dE}{\sqrt{E^2 - \Delta_i(T)^2}} \right]. \quad (2)$$

Here $f = [1 + \exp(E/k_B T)]^{-1}$ is the Fermi function, $\Delta_i(T) = \Delta_{0,i} \tanh\{1.82[1.018(T_c/T - 1)]^{0.51}\}$,⁴⁴ and I_i is the contribution of the i -th gap to $\lambda_{ab}^{-2}(T = 0)$, which is obtained as:⁴⁰

$$I_i = \frac{e^2}{2\pi\epsilon_0 c^2 h L_c} \oint_{i\text{-th band}} v_{F,i}(\mathbf{k}) d\mathbf{k}. \quad (3)$$

Here e is the elementary charge, ϵ_0 is the electric constant, h is the Planck constant, c is the speed of light, L_c is the c -axis lattice parameter and \mathbf{k} is a momentum vector within the reciprocal space. Integrations are made over the corresponding Fermi surface contours.

The analysis reveals that the four bands observed in the ARPES experiment alone do not describe the experimentally measured $\lambda_{ab}^{-2}(T)$. In analogy with the above discussed $\xi_{ab}(H_{\text{ap}})$ results [see Fig. 2 (c)] the presence

of additional bands with smaller superconducting energy gaps are needed. The difference between the calculated and measured λ_{ab}^{-2} allows access to the zero-temperature value of the superconducting gap of the ϵ -bands. A reasonably good agreement is achieved for $\Delta_{0,\epsilon} \simeq 2.4(2)$ meV, $\lambda_{ab, \text{ARPES}}(0) \simeq 187(11)$ nm and a contribution to the zero-temperature superfluid density $[\lambda_{ab,\epsilon}^{-2}(0)/\lambda_{ab}^{-2}(0)]$ of $\simeq 37(4)\%$ [see Fig. 4 (a), Table I and the Supplemental Information for details, Ref. 18]. With the known value of the Fermi velocity $\langle v_F \rangle_\epsilon \simeq 0.025$ eV·nm (see Table I), a sum of the diameters of additional bands $\langle d_F \rangle_\epsilon \simeq 10.0$ nm⁻¹ was found. Two important points need to be mentioned. (i) The data in Fig. 4a were analyzed using only three independent parameters [$\Delta_{0,\epsilon}$, $\langle d_F \rangle_\epsilon$ and $n = \lambda_{ab, \text{ARPES}}(0)/\lambda_{ab, \mu\text{SR}}(0)$]. The rest of the parameters were fixed to the values obtained in ARPES, magnetization and $\xi_{ab}(H_{\text{ap}})$ measurements [see Fig. 2 (c), Ref. 7 and Table I]. (ii) The zero temperature value of the in-plane penetration depth calculated from the ARPES data (including contribution of ϵ -bands) results in $\lambda_{ab, \text{ARPES}}(0) \simeq 187(11)$ nm, which is approximately 10% lower than 208(4) nm as determined by the μSR experiment. Note that a similar difference was reported for Ba_{1-x}K_xFe₂As₂ in Refs. 40,42.

Temperature dependencies of the superfluid density components of α -, β -, γ - and δ -bands follow the BCS type of mean-field behaviour, while the response of ϵ -bands is markedly different (see Fig. 3 in the Supplemental Information, Ref. 18). This may suggest that ϵ -bands are only weakly involved into superconductivity, and alone would have T_c of the order of 15 K only. Above 15 K the superconductivity in ϵ -bands remains due to effects of interband coupling.^{45,46}

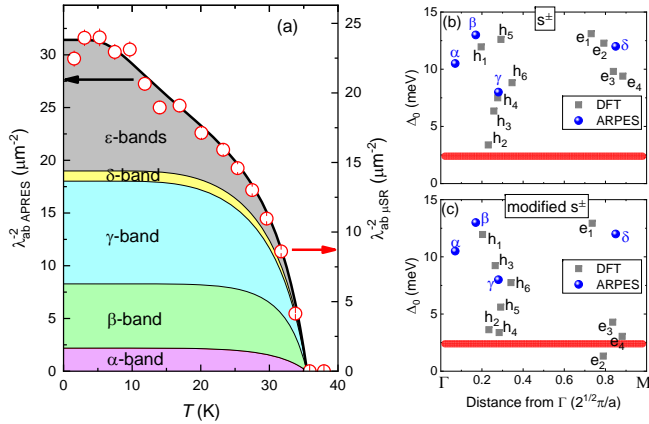


FIG. 4: (a) $\lambda_{ab}^{-2}(T)$ obtained from the measured $\langle B^2 \rangle^{1/2}$ at $\mu_0 H = 11$ mT ($\lambda_{ab, \mu\text{SR}}^{-2}$) and inferred from ARPES data ($\lambda_{ab, \text{ARPES}}^{-2}$). The colored stripes are contributions of various Fermi surfaces to $\lambda_{ab}^{-2}(T)$. (b) Gaps as a function of momentum distance from Γ in hole (h) and electron (e) pockets as obtained from DFT calculations within the framework of the s^\pm -model.¹³ (c) the same as in (b) but for a modified s^\pm -model. The red line is $\Delta_0 = 2.4$ meV. The blue points refer to the ARPES values.⁸

The s^\pm gap symmetry, with a sign change between hole and electron pockets, in CaKFe₄As₄ was supported by the observation of the neutron-spin resonance peak with a characteristic energy $\simeq 12.5$ meV at the antiferromagnetic wave vector $\mathbf{Q}_{\text{AF}} = (\pi, \pi)$.^{47,48} We should emphasize, however that the recent DFT calculations obtain two stable solutions for possible gap functions in CaKFe₄As₄. The first corresponds to the conventional s^\pm -state, while the second (modified s^\pm -state) allows an additional sign change within the hole and electron pockets with some gaps being small in magnitude.¹³ The modified s^\pm -state enhances the spin response at the antiferromagnetic wave vector (π, π) and, therefore, becomes consistent with the results of Iida *et al.*⁴⁷ This enhancement, however, cannot be regarded as a pure spin resonance due to relatively small gap sizes on some electron and hole pocket bands. As a consequence, the resonance in CaKFe₄As₄ cannot be treated as a true spin excitation, since its position is not *below* but *inside* the particle-hole continuum (see the Supplemental Information for details, Ref. 18).

Figures 4 (b) and (c) show the superconducting gaps in hole (h) and electron (e) pockets as a function of momentum distance from the Γ point (the center of the Brillouin zone) as obtained from DFT calculations within the framework of the s^\pm and modified s^\pm models, respectively.¹³ Within the s^\pm approach only one out of ten bands has the gap value smaller than 5 meV [Fig. 4 (b)]. Note, that due to the so-called red/blue shift, reported by the authors of Ref. 13, one can not rely on the band diameters obtained from the DFT calculations, so the analysis similar to the one made above for obtaining $\lambda_{ab, \text{ARPES}}^{-2}(T)$ can not be performed. One would expect, however, that the contribution of 9 bands to $\lambda_{ab}^{-2}(T)$ should be at least twice as high as for 4 bands obtained in ARPES experiments [see Fig. 4 (a)]. This would lead to complete disagreement between the calculated and experimentally measured $\lambda_{ab}^{-2}(T)$ dependencies. In contrast, within the modified s^\pm -model 5 (2 hole and 3 electron) bands have gap values close to $\Delta_0 = 2.4$ meV [Fig. 4 (c)]. They may account, therefore, for 37% contribution to $\lambda_{ab}^{-2}(0)$ (see Table I). The other 5 bands left (4 hole and 1 electron band) result in gap values comparable with that obtained in ARPES experiments. This implies that the modified s^\pm -model agrees better with our experimental findings.

To conclude, the temperature and the magnetic field dependencies of the in-plane magnetic penetration depth λ_{ab} and the field dependence of the vortex core size ξ_{ab} in CaKFe₄As₄ single crystal were studied by means of muon-spin rotation. A comparison of the temperature dependence of λ_{ab}^{-2} measured by μSR to the one determined from ARPES experiments confirms the presence of multiple gaps at the Fermi level. An agreement between the μSR and ARPES data requires the presence of additional bands which are characterised by small superconducting gaps with an averaged zero-temperature value of $\Delta_0 \simeq 2.4(2)$ meV. Our data suggest that the order parameter in CaKFe₄As₄ may acquire a more complex form

than the simple s^{\pm} -symmetry. The gap sign change occurs not just between the electron and hole pockets but also within pockets of similar type. Such a gap state is favored by weakened interband repulsion and yields further interesting consequences for the spin resonance, which needs to be further verified experimentally

The work was performed at the Swiss Muon Source ($S\mu S$), Paul Scherrer Institute (PSI, Switzerland). RK acknowledges D.V. Evtushinsky for helpful discussions

and J. Barker for help with the manuscript preparation. WRM was funded by the Gordon and Betty Moore Foundation EPIQS Initiative through Grant GBMF4411. Work at Ames Laboratory was supported by the U.S. Department of Energy, Office of Science, Basic Energy Sciences, Materials Science and Engineering Division. Ames Laboratory is operated for the U.S. DOE by Iowa State University under Contract No. DE-AC02-07CH11358.

-
- * Electronic address: rustem.khasanov@psi.ch
- ¹ Y. Kamihara, T. Watanabe, M. Hirano, and H. Hosono, *J. Am. Chem. Soc.* **130**, 3296 (2008).
 - ² F.-C. Hsu, J.-Y. Luo, K.-W. Yeh, T.-K. Chen, T.-W. Huang, P. M. Wu, Y.-C. Lee, Y.-L. Huang, Y.-Y. Chu, D.-C. Yan, and M.-K. Wu, *Proc. Natl. Acad. Sci. USA* **105**, 14262 (2008).
 - ³ G. R. Stewart, *Rev. Mod. Phys.* **83**, 1589 (2011).
 - ⁴ X. Chen, P. Dai, D. Feng, T. Xiang, and F. C. Zhang, *Nat. Sci. Rev.* **1**, 371 (2014).
 - ⁵ J. Paglione and R. L. Greene, *Nat. Phys.* **6**, 645 (2010).
 - ⁶ A. Iyo, K. Kawashima, T. Kinjo, T. Nishio, S. Ishida, H. Fujihisa, Y. Gotoh, K. Kihou, H. Eisaki, and Y. Yoshida, *J. Am. Chem. Soc.* **138**, 3410 (2016).
 - ⁷ W. R. Meier, T. Kong, U. S. Kaluarachchi, V. Taufour, N. H. Jo, G. Drachuck, A. E. Böhmer, S. M. Saunders, A. Sapkota, A. Kreyssig, M. A. Tanatar, R. Prozorov, A. I. Goldman, F. F. Balakirev, A. Gurevich, S. L. Bud'ko, and P. C. Canfield, *Phys. Rev. B* **94**, 064501 (2016).
 - ⁸ D. Mou, T. Kong, W. R. Meier, F. Lochner, L.-L. Wang, Q. Lin, Y. Wu, S. L. Bud'ko, I. Eremin, D. D. Johnson, P. C. Canfield, and A. Kaminski, *Phys. Rev. Lett.* **117**, 277001 (2016).
 - ⁹ K. Cho, A. Fente, S. Teknowijoyo, M. A. Tanatar, K. R. Joshi, N. M. Nusran, T. Kong, W. R. Meier, U. Kaluarachchi, I. Guillamón, H. Suderow, S. L. Bud'ko, P. C. Canfield, and R. Prozorov, *Phys. Rev. B* **95**, 100502(R) (2017).
 - ¹⁰ A. Fente, W. R. Meier, T. Kong, V. G. Kogan, S. L. Bud'ko, P. C. Canfield, I. Guillamon, H. Suderow, *arXiv:1608.00605*.
 - ¹¹ J. Cui, Q.-P. Ding, W. R. Meier, A. E. Böhmer, T. Kong, V. Borisov, Y. Lee, S. L. Bud'ko, R. Valentí, P. C. Canfield, Y. Furukawa, *Phys. Rev. B* **96**, 104512 (2017).
 - ¹² P. K. Biswas, A. Iyo, Y. Yoshida, H. Eisaki, K. Kawashima, and A. D. Hillier, *Phys. Rev. B* **95**, 140505(R) (2017).
 - ¹³ F. Lochner, F. Ahn, T. Hickel, and I. Eremin, *Phys. Rev. B* **96**, 094521 (2017).
 - ¹⁴ A. Amato, H. Luetkens, K. Sedlak, A. Stoykov, R. Scheuermann, M. Elender, A. Raselli, and D. Graf, *Review of Scientific Instruments* **88**, 093301 (2017).
 - ¹⁵ R. Khasanov, H. Zhou, A. Amato, Z. Guguchia, E. Morenzoni, X. Dong, G. Zhang, and Z.-X. Zhao *Phys. Rev. B* **93**, 224512 (2016).
 - ¹⁶ A. Suter and B. M. Wojek, *Phys. Procedia* **30**, 69 (2012).
 - ¹⁷ A. Maisuradze, R. Khasanov, A. Shengelaya, and H. Keller, *J. Phys.: Condens. Matter* **21**, 075701 (2009).
 - ¹⁸ See Supplemental Information at <http://link.aps.org/supplemental/xxxxx> for description of the experimental techniques and the data analysis procedure, which includes Ref. 19–23.
 - ¹⁹ R. Jiang, D. Mou, Y. Wu, L. Huang, C. D. McMillen, J. Kolis, H. G. Giesber, J. J. Egan, and A. Kaminski, *Review of Scientific Instruments* **85**, 033902 (2014).
 - ²⁰ R. Khasanov, D. G. Eshchenko, D. Di Castro, A. Shengelaya, F. La Mattina, A. Maisuradze, C. Baines, H. Luetkens, J. Karpinski, S. M. Kazakov, and H. Keller, *Phys. Rev. B* **72**, 104504 (2005).
 - ²¹ T. M. Riseman, J. H. Brewer, K. H. Chow, W. N. Hardy, R. F. Kiefl, S. R. Kreitzman, R. Liang, W. A. MacFarlane, P. Mendels, G. D. Morris, J. Rammer, J. W. Schneider, C. Niedermayer, and S. L. Lee, *Phys. Rev. B* **52**, 10569 (1995).
 - ²² F. Ahn, I. Eremin, J. Knolle, V. B. Zabolotnyy, S. V. Borisenko, B. Büchner, and A. V. Chubukov, *Phys. Rev. B* **89**, 144513 (2014).
 - ²³ N. Qureshi, P. Steffens, D. Lamago, Y. Sidis, O. Sobolev, R. A. Ewings, L. Harnagea, S. Wurmehl, B. Büchner, and M. Braden, *Phys. Rev. B* **90**, 144503 (2014).
 - ²⁴ R. Khasanov, I. L. Landau, C. Baines, F. La Mattina, A. Maisuradze, K. Togano, and H. Keller *Phys. Rev. B* **73**, 214528 (2006).
 - ²⁵ R. Khasanov, A. Shengelaya, A. Maisuradze, F. La Mattina, A. Bussmann-Holder, H. Keller, and K. A. Müller *Phys. Rev. Lett.* **98**, 057007 (2007).
 - ²⁶ M. Weber, A. Amato, F. N. Gygax, A. Schenck, H. Maletta, V. N. Duginov, V. G. Grebinnik, A. B. Lazarev, V. G. Olshevsky, V. Yu. Pomjakushin, S. N. Shilov, V. A. Zhukov, B. F. Kirillov, A. V. Pirogov, A. N. Ponamarev, V. G. Storchak, S. Kapusta, and J. Bock, *Phys. Rev. B* **48**, 13022 (1993).
 - ²⁷ E. H. Brandt, *Phys. Rev. B* **37**, 2349(R) (1988).
 - ²⁸ E. H. Brandt, *Phys. Rev. B* **68**, 054506 (2003).
 - ²⁹ S. L. Lee, P. Zimmermann, H. Keller, M. Warden, I. M. Savić, R. Schauwecker, D. Zech, R. Cubitt, E. M. Forgan, P. H. Kes, T. W. Li, A. A. Menovsky, and Z. Tarnawski, *Phys. Rev. Lett.* **71**, 3862 (1993).
 - ³⁰ C. M. Aegerter, J. Hofer, I. M. Savić, H. Keller, S. L. Lee, C. Ager, S. H. Lloyd, and E. M. Forgan *Phys. Rev. B* **57**, 1253 (1998).
 - ³¹ E. H. Brandt, *J. Low Temp. Phys.* **26**, 709 (1977).
 - ³² E. H. Brandt, *J. Low Temp. Phys.* **73**, 355 (1988).
 - ³³ J. Rammer, *Physica C* **177**, 421 (1991).
 - ³⁴ R. Kadono, *J. Phys.: Condens. Matter* **16**, S4421 (2004).
 - ³⁵ J. E. Sonier, J. H. Brewer, and R. F. Kiefl, *Rev. Mod. Phys.* **72**, 769 (2000).
 - ³⁶ J. E. Sonier, *J. Phys.: Condens. Matter* **16**, S4499 (2004).
 - ³⁷ V. G. Kogan, R. Prozorov, S. L. Bud'ko, P. C. Canfield, J. R. Thompson, J. Karpinski, N. D. Zhigadlo, P. Miranović, *Phys. Rev. B* **74**, 184521 (2006).
 - ³⁸ A. Fente, E. Herrera, I. Guillamon, H. Suderow, S. Manas-

- Valero, M. Galbiati, E. Coronado, and V. G. Kogan, Phys. Rev. B **94**, 014517 (2016)
- ³⁹ M. R. Eskildsen, M. Kugler, S. Tanaka, J. Jun, S. M. Kazakov, J. Karpinski, and Ø. Fischer, Phys. Rev. Lett. **89**, 187003 (2002).
- ⁴⁰ D.V. Evtushinsky, D.S. Inosov, V.B. Zabolotnyy, M.S. Viazovska, R. Khasanov, A. Amato, H.-H. Klauss, H. Luetkens, Ch. Niedermayer, G.L. Sun, V. Hinkov, C.T. Lin, A. Varykhalov, A. Koitzsch, M. Knupfer, B. Büchner, A.A. Kordyuk, and S.V. Borisenko, New Journal of Physics, **11**, 055069 (2009).
- ⁴¹ M. Tinkham, *Introduction to Superconductivity* (Krieger Publishing company, Malabar, Florida, 1975).
- ⁴² R. Khasanov, D. V. Evtushinsky, A. Amato, H.-H. Klauss, H. Luetkens, Ch. Niedermayer, B. Büchner, G. L. Sun, C. T. Lin, J. T. Park, D. S. Inosov, and V. Hinkov Phys. Rev. Lett. **102**, 187005 (2009).
- ⁴³ R. Khasanov, A. Shengelaya, A. Maisuradze, F. La Martina, A. Bussmann-Holder, H. Keller, and K.A. Müller, Phys. Rev. Lett. **98**, 057007 (2007).
- ⁴⁴ A. Carrington and F. Manzano, Physica C **385**, 205 (2003).
- ⁴⁵ H. Suhl, B.T. Matthias, and L.R. Walker, Phys. Rev. Lett. **3**, 552 (1959).
- ⁴⁶ V.A. Moskalenko, Phys. Met. Metallogr **8**, 25 (1958).
- ⁴⁷ K. Iida, M. Ishikado, Y. Nagai, H. Yoshida, A. D. Christianson, N. Murai, K. Kawashima, Y. Yoshida, H. Eisaki, and A. Iyo, J. Phys. Soc. Jpn. **86**, 093703 (2017).
- ⁴⁸ $\mathbf{Q}_{AF} = (\pi, \pi)$ corresponds to the $\text{CaKFe}_4\text{As}_4$ Brillouin zone. It is typically equal to $(\pi, 0)$ for most of Fe-SC's.